2015

Mitochondrial dysfunction and loss of glutamate uptake in primary astrocytes exposed to titanium dioxide nanoparticles

Christina L. Wilson
University of Nebraska-Lincoln

Vaishaali Natarajan
University of Nebraska-Lincoln, vaishaali.n@gmail.com

Stephen L. Hayward
University of Nebraska-Lincoln, stephen.hayward@unl.edu

Oleh Khalimonchuk
University of Nebraska-Lincoln, okhalimonchuk2@unl.edu

Srivatsan Kidambi
New York Methodist Hospital, skidambi2@unl.edu

Volume 7 | Number 44 | 28 November 2015 | Pages 18347–18828

Nanoscale

www.rsc.org/nanoscale

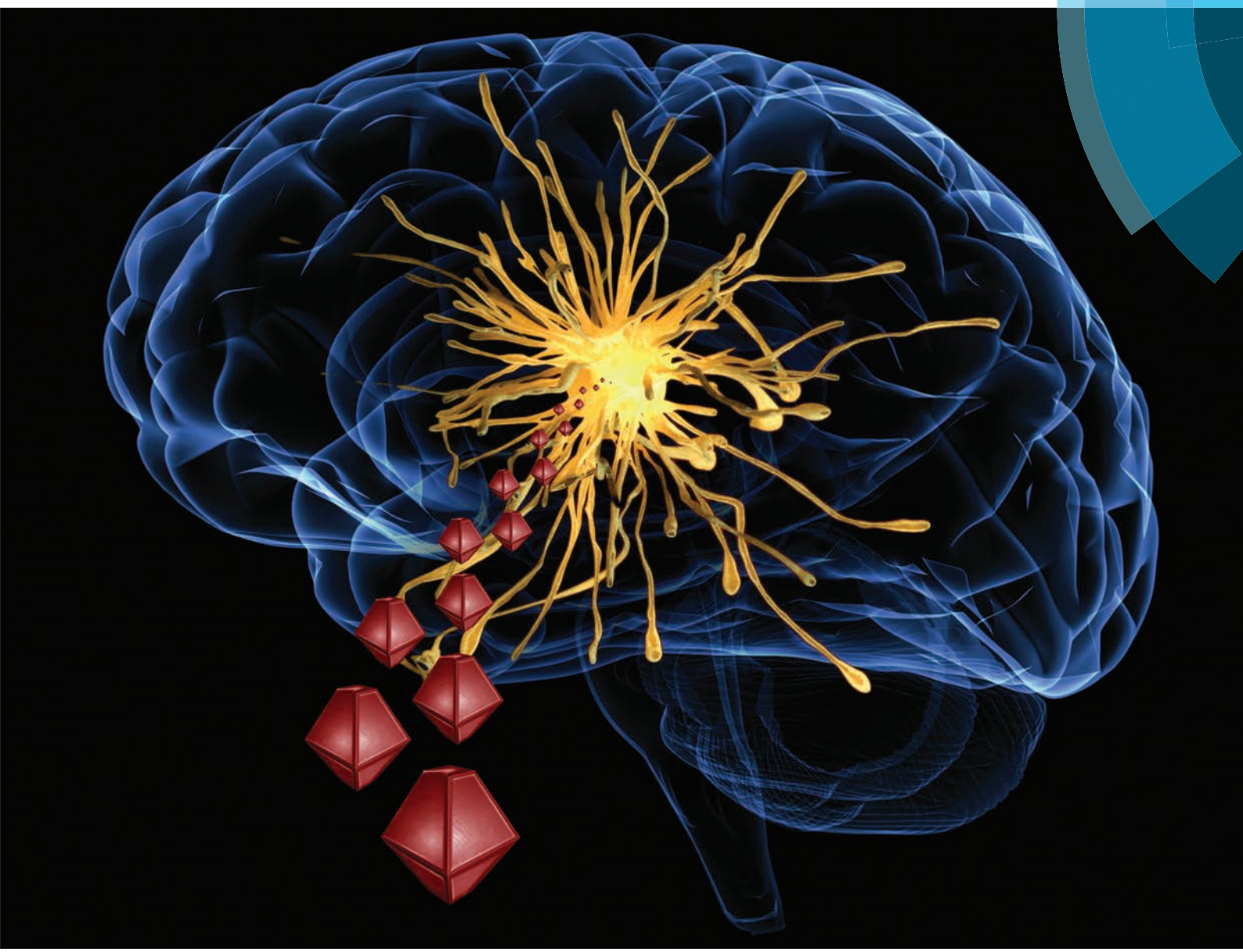

ISSN 2040-3364

ROYAL SOCIETY OF CHEMISTRY

PAPER

Srivatsan Kidambi *et al.*

Mitochondrial dysfunction and loss of glutamate uptake in primary astrocytes exposed to titanium dioxide nanoparticles

NCNST

Nanoscale

PAPER

View Article Online
View Journal | View Issue

Cite this: *Nanoscale*, 2015, **7**, 18477

Mitochondrial dysfunction and loss of glutamate uptake in primary astrocytes exposed to titanium dioxide nanoparticles†

Christina L. Wilson,[a] Vaishaali Natarajan,[a] Stephen L. Hayward,[a] Oleh Khalimonchuk[b] and Srivatsan Kidambi*[a,c,d]

Titanium dioxide (TiO_2) nanoparticles are currently the second most produced engineered nanomaterial in the world with vast usage in consumer products leading to recurrent human exposure. Animal studies indicate significant nanoparticle accumulation in the brain while cellular toxicity studies demonstrate negative effects on neuronal cell viability and function. However, the toxicological effects of nanoparticles on astrocytes, the most abundant cells in the brain, have not been extensively investigated. Therefore, we determined the sub-toxic effect of three different TiO_2 nanoparticles (rutile, anatase and commercially available P25 TiO_2 nanoparticles) on primary rat cortical astrocytes. We evaluated some events related to astrocyte functions and mitochondrial dysregulation: (1) glutamate uptake; (2) redox signaling mechanisms by measuring ROS production; (3) the expression patterns of dynamin-related proteins (DRPs) and mitofusins 1 and 2, whose expression is central to mitochondrial dynamics; and (4) mitochondrial morphology by MitoTracker® Red CMXRos staining. Anatase, rutile and P25 were found to have LC_{50} values of 88.22 ± 10.56 ppm, 136.0 ± 31.73 ppm and 62.37 ± 9.06 ppm respectively indicating nanoparticle specific toxicity. All three TiO_2 nanoparticles induced a significant loss in glutamate uptake indicative of a loss in vital astrocyte function. TiO_2 nanoparticles also induced an increase in reactive oxygen species generation, and a decrease in mitochondrial membrane potential, suggesting mitochondrial damage. TiO_2 nanoparticle exposure altered expression patterns of DRPs at low concentrations (25 ppm) and apoptotic fission at high concentrations (100 ppm). TiO_2 nanoparticle exposure also resulted in changes to mitochondrial morphology confirmed by mitochondrial staining. Collectively, our data provide compelling evidence that TiO_2 nanoparticle exposure has potential implications in astrocyte-mediated neurological dysfunction.

Received 2nd June 2015,
Accepted 28th July 2015

DOI: 10.1039/c5nr03646a

www.rsc.org/nanoscale

1. Introduction

Titanium dioxide (TiO_2) nanoparticles are the second most produced engineered nanomaterial in the world with a vast majority utilized in cosmetics, including sunscreens, and other consumer products.[1,2] The unique properties of TiO_2 nanoparticles have also proven useful in applications of air and water purification and energy storage providing increased opportunities for commercial and industrial exposure to these nanoparticles.[3] This increased human and environmental exposure to TiO_2 nanoparticles has led to an intense scrutiny of its biocompatibility resulting in many animal and *in vitro* studies that suggests a need for concern.[4–6] Wang and co-workers demonstrated that a single oral administration of TiO_2 nanoparticles in rats caused nanoparticle distribution and accumulation in various tissues including the brain.[7] Intranasal exposure of TiO_2 nanoparticles also demonstrated high accumulation of the nanoparticles in different regions of the brain resulting in increase of glial fibrillary acidic protein (GFAP) positive cells, oxidative stress, and brain tissue damage.[8] Wu and co-workers exposed TiO_2 nanoparticles to PC12 cell lines and observed decreased cell viability, generation of reactive oxygen species (ROS), loss of mitochondrial membrane potential (MMP) and increased expression of biomarkers associated with apoptosis per cell death.[9] Long *et al.* demonstrated a cell-dependent effect due to exposure to TiO_2

[a]*Department of Chemical and Biomolecular Engineering, University of Nebraska-Lincoln, NE 68588, USA. E-mail: skidambi2@unl.edu*
[b]*Department of Biochemistry and Nebraska Redox Biology Center, University of Nebraska-Lincoln, NE 68588, USA*
[c]*Nebraska Center for Materials and Nanoscience, University of Nebraska-Lincoln, NE 68588, USA*
[d]*Mary and Dick Holland Regenerative Medicine Program, University of Nebraska Medical Center, NE 68198, USA*
†Electronic supplementary information (ESI) available. See DOI: 10.1039/c5nr03646a

nanoparticles wherein BV2 microglia cell lines had a faster decrease in viability compared to N27 neuronal cell lines suggesting that microglia are more susceptible to TiO_2 nanoparticles.[10] Together, these *in vitro* and *in vivo* studies indicate that exposure to TiO_2 nanoparticles result in a certain degree of nanoparticle accumulation and toxicity. However, the majority of these studies have focused on neurons and neuronal cell lines leaving a significant gap of knowledge regarding toxicity mechanisms in other brain cells including astrocytes.

Astrocytes are the most abundant cell type in the brain; they are intimately associated with synapses and govern key steps in synapse formation and plasticity. Glutamate homeostasis is maintained by neuron–astrocyte interaction *via* several glutamate transporters and is a key metabolic function of astrocytes and neurons at the mitochondrial level.[11–14] Numerous studies have revealed that astrocytes release neuroactive substances, called gliotransmitters, including glutamate, GABA, ATP/adenosine, or D-serine.[15–19] These gliotransmitters activate receptors in neurons, exerting diverse and complex cellular effects that result in the regulation of the neuronal excitability, synaptic transmission and plasticity, and neural network function. The increasing interest in identification of astrocytes' roles in regulating brain function has led to great excitement regarding their potential impact on prospective therapeutics for neurological conditions. Hence, astrocytes might possess the key to understand the underlying mechanisms that mediate brain injury due to exposure to TiO_2 nanoparticles. Furthermore, all the vital roles of astrocytes in brain function are largely energy dependent and recent reports have indicated that high doses of TiO_2 nanoparticles induce significant mitochondrial injury and alter the bioenergetic function of mitochondria.[20,21] Thus, it is critical to understand the mechanisms of toxicity in astrocytes, especially in regard to mitochondrial health.

Mitochondria are essential bioenergetic organelles that exploit a highly dynamic nature to participate in several processes vital to meet the energy requirements of the cell. The constant balance of merging (fusion) and dividing (fission) maintains the mitochondrial dynamics facilitating cell bioenergetic demands and eliminating injured mitochondria thereby assuring sufficient energy supply for proper cell function. Fusion, mediated by membrane-anchored dynamin family members mitofusins (Mfn 1 and 2), is required for mitochondrial (mt) DNA maintenance because it allows mtDNA exchange and protects the mtDNA from damage during stress.[22,23] Fission, mediated by cytosolic dynamin family member dynamin-related protein 1 (Drp1), is essential for mitochondrial distribution and selective elimination of damaged mtDNA. Mitochondria utilize fission in response to extensive and persistent mitochondrial damage, as abundant fission can result in the release of factors to initiate the cascade for cellular apoptosis.[24] The endocytosis and interaction with mitochondria of TiO_2 nanoparticles have been confirmed by previous studies, however these studies have not ventured into mechanisms of toxicity beyond ROS generation, anti-oxidant response and MMP disruption leaving a gap in the current toxicity knowledge base.[25,26]

In this study we sought to assess the impact of low concentrations of TiO_2 nanoparticles on cellular activity of primary cortical astrocytes. We utilized three commercially employed TiO_2 nanoparticles (P25, anatase, and rutile), to investigate nanoparticle specific perturbation in an explicit range of concentrations mimicking TiO_2 nanoparticle accumulation. Additionally, we evaluated the effect of TiO_2 nanoparticle exposure on mitochondrial health and ROS production, indicators of perturbations in normal brain function. Our findings demonstrate toxic effects of TiO_2 nanoparticles on cellular and mitochondrial function in primary astrocytes and suggest that mitochondrial stress can be used as an early and potent diagnostic marker for nanotoxicological inquiries.

2. Results and discussion

2.1. TiO_2 nanoparticle characterization

In this study, we utilized three different TiO_2 nanoparticles (P25, anatase and rutile), due to their unique crystal structures and abundance in commercial products, and performed extensive nanoparticle characterization using transmission electron microscopy (TEM) and dynamic light scattering (DLS). TiO_2 nanoparticle characterization is a vital part of understanding and interpreting the toxic potential of nanoparticles. Furthermore, nanoparticle size and crystalline structure have been studied as underlying characteristics for nanoparticle toxicity.[27–30] TEM images demonstrated that anatase TiO_2 nanoparticles had a characteristic spherical crystal structure while rutile nanoparticles had a typical rod-like crystal structure (Fig. 1). The anatase and rutile TiO_2 nanoparticles utilized for this study were both reported to be 50 nm in diameter by the manufacturer, thus allowing for observations of crystal structure influence on nanoparticle toxicity independent of the particle size. This was important as many studies comparing pure phase rutile and anatase nanoparticles utilize different sized nanoparticles thus not eliminating the effect of the nanoparticle size on toxicity. The commercially used P25 nanoparticles were the third variation of TiO_2 nanoparticles that contained a 3 : 1 mixture of anatase and rutile, have structural characteristics of both anatase and rutile and were reported to be 21 nm in diameter.

We further performed DLS and zeta potential analysis to investigate the behavior of the particles in media used for culturing astrocytes. Previous reports have shown that nanoparticles agglomerate in cell culture media.[30–33] To compare the level of agglomeration of the TiO_2 nanoparticles under physiologically relevant conditions, in the presence of proteins and divalent ions, we studied the agglomeration of the TiO_2 nanoparticles in serum containing astrocyte culture media. Nanoparticle suspensions were prepared in astrocytes media in the same manner as for the cell culture studies. The nanoparticle suspensions were then characterized using DLS for hydrodynamic diameter of the aggregates and zeta potential to

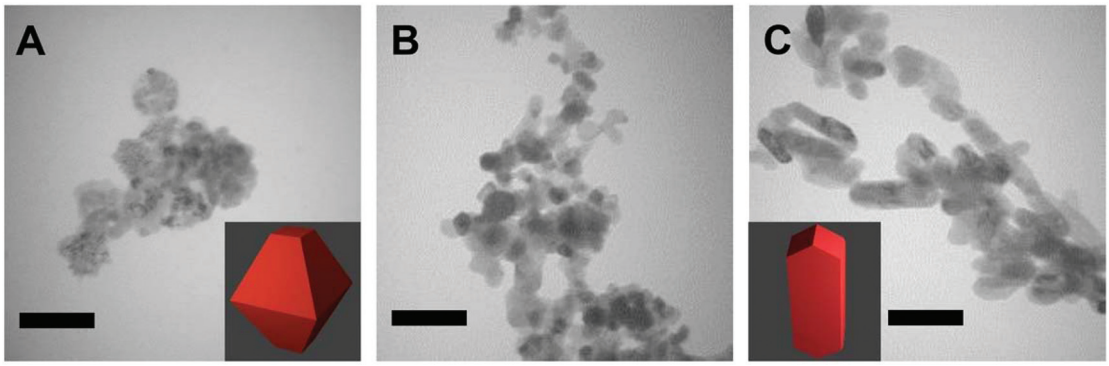

Fig. 1 Physical characterization of TiO_2 nanoparticles. TEM images of anatase (A), P25 (B), and rutile (C). Scale bar = 100 nm.

discern nanoparticle charge and colloidal stability. As shown in Table 1, P25, anatase, and rutile nanoparticles aggregated to an average diameter of approximately 360 nm, 540 nm, and 360 nm, respectively. We observed that the average hydrodynamic diameter had crystalline form dependence, but not a concentration dependence indicating that the relative concentrations would be reliable for our study. The type of crystal structure of the particles (anatase *vs.* rutile) and the relative composition of the three forms of nanoparticles might attribute to the observed variations in their aggregation size considering varied interaction with media components.[34] Zeta potential was also measured for the three TiO_2 nanoparticles (Table 1). The zeta potential values did not significantly change in the three forms of the nanoparticles and in all three concentrations. In all cases the weakly negative net charge of the nanoparticles highlighted their inherent colloidal instability driven by favorable aggregation forces. Our extensive characterization provides us with valuable information about the intricate characteristics of the nanoparticles, including size, charge and driving forces for aggregation, that elicits valuable insight for data analysis and comparison with previous studies.

Table 1 Physical characterization of TiO_2 nanoparticles. Hydrodynamic diameter and zeta potential measured in culture media. Data are expressed as the mean ± standard deviation of two independent samples

	Size		Astrocyte culture media[a]	
Nanoparticle	(nm)	ppm	Hydrodynamic diameter (nm)	Zeta potential (mV)
P25 (70% anatase & 30% rutile)	~21	25	374.3 ± 26.4	−10.7 ± 4.6
		50	367.6 ± 15.3	−8.5 ± 4.9
		100	337.9 ± 14.7	−9.2 ± 4.3
Rutile	~50	25	366.9 ± 15.0	−11.4 ± 6.2
		50	363.5 ± 19.2	−12.1 ± 3.6
		100	362.4 ± 18.4	−8.1 ± 3.4
Anatase	~50	25	541.2 ± 51.0	−10.4 ± 5.0
		50	555.9 ± 41.3	−9.4 ± 4.1
		100	545.3 ± 47.8	−10.8 ± 3.2

[a] Composition includes 10% heat inactivated horse serum, 1% 1 M hepes buffer, 1% L-glutamine, and 1% penicillin–streptomycin in DMEM.

2.2. TiO_2 nanoparticles cytotoxicity to primary astrocytes

We determined the concentrations of acute toxicity to primary rat cortical astrocytes using lethal concentration assay by exposing primary astrocytes to different concentrations of the three TiO_2 nanoparticles for 24 h. As seen in Table 2 and ESI Fig. 1,† the LC_{50} values of P25, anatase and rutile TiO_2 nanoparticles were 62.37 ± 9.06 ppm, 88.22 ± 10.56 ppm, and 136.0 ± 31.73 ppm, respectively. Our results are in agreement with other studies indicating that the anatase crystalline phase is more toxic than rutile.[9] This result provided us with a concentration range of acute toxicity to investigate the underlying mechanistic perturbation induced by the gradual accumulation of nanoparticles in brain observed akin to animal models.[7,8,35] Therefore, all subsequent mechanistic studies were carried out using three different concentrations of TiO_2 nanoparticles (25 ppm, 50 ppm, and 100 ppm) with 24 h exposure that is reflective of the LC_{50} data. These concentrations are in the relevant sub-acute toxicity range, as compared to previous studies that have been carried out using higher concentrations and were thus unable to discern mechanistic response beyond loss of viability.[36,37] Two recent studies have employed lower concentrations to delineate the toxicity mechanisms on brain cells, however these studies are limited as they use cell lines and lack understanding with regard to the TiO_2 effect on mitochondria.[9,38] Cell lines are commonly utilized in toxicity studies due to ease of culture and stability of phenotype over multiple passages, however,

Table 2 Lethal concentration summary table. Lethal concentration was quantified at 0 ppm, 25 ppm, 50 ppm, 100 ppm, 300 ppm, 500 ppm, 700 ppm, and 1000 ppm nanoparticle (ESI Fig. 1). P25 was observed to be the most lethal nanoparticle after 24 h treatment followed by anatase and rutile as determined by calculating the LC_{50} utilizing sigma plot analysis. $N = 6$

Nanoparticle	LC_{50} value (ppm)
P25	62.37 ± 9.06
Anatase	88.22 ± 10.56
Rutile	136.0 ± 31.73

the immortalization process often causes physiological differences when compared to cells *in vivo*.[39] In our study, we utilized primary astrocytes isolated from the rat brain, which are generally recognized as a better *in vivo* mimic of the cells. These studies provide basis for the TiO_2 nanoparticle toxic effect, however, the effect of TiO_2 nanoparticles on mitochondria, and essential bioenergetic organelles, is largely unexplored. Therefore, the main goal of our study is to further probe the effect of TiO_2 nanoparticle on primary astrocytes focusing on the changes in mitochondrial dynamics and function.

2.3. TiO_2 nanoparticle and astrocytes viability

To study the effect of TiO_2 nanoparticles on the primary astrocyte morphology and viability, we utilized phase images and the MTT assay (Fig. 2). Changes in the astrocyte morphology represent a strong qualitative indicator and the MTT assay is a

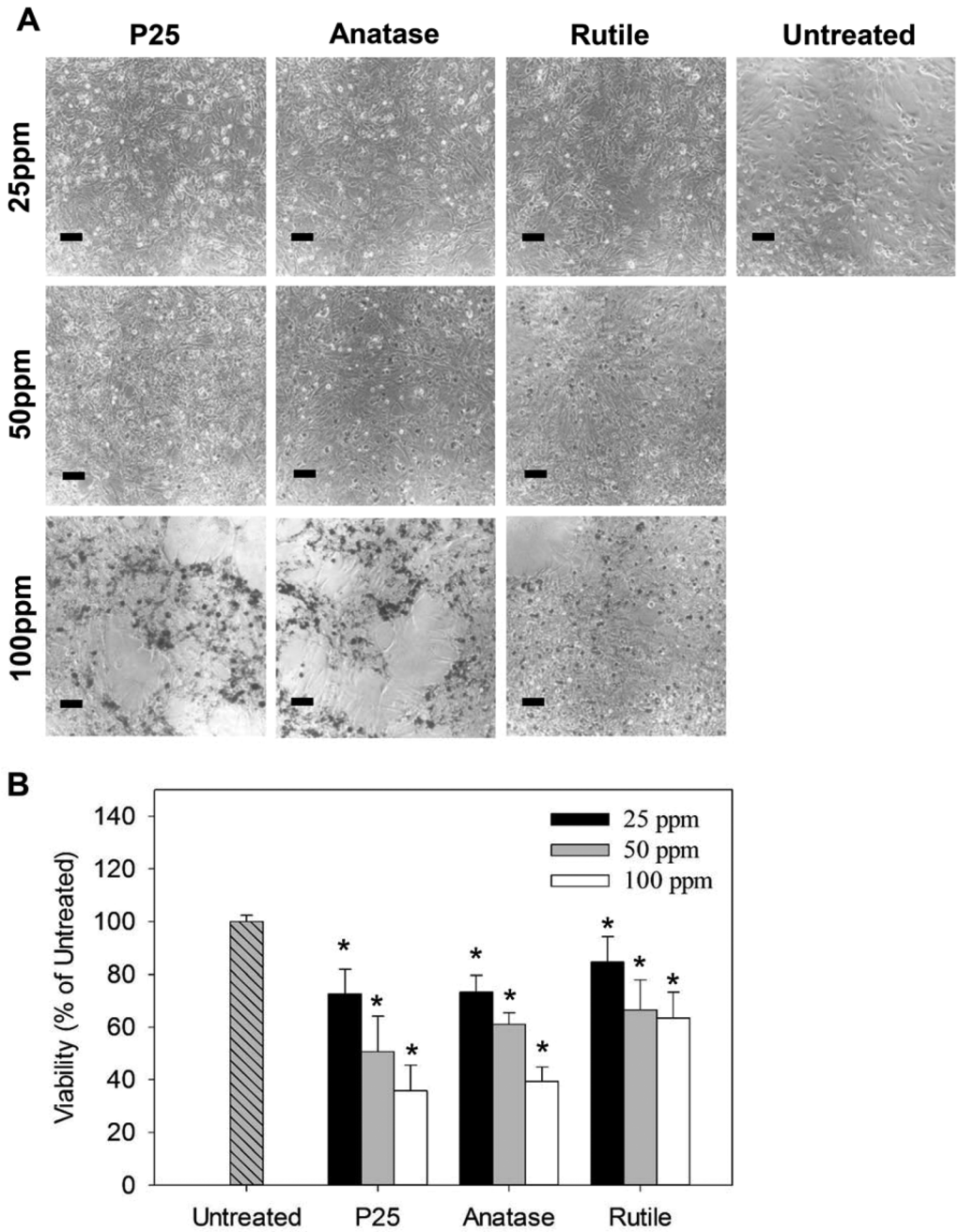

Fig. 2 Effect of TiO_2 nanoparticles on morphology and viability of astrocytes. A concentration- and form-dependent loss in morphology and viability was observed by phase images (A) and MTT assay (B) after 24 h exposure. P25 and anatase 100 ppm treated astrocytes exhibited the greatest loss (65% and 61% decrease, respectively) in viability and exposure to rutile 100 ppm TiO_2 nanoparticles resulted in a lesser decrease (37%). In all three nanoparticles, cells treated with 25 ppm and 50 ppm show much less change in morphology than 100 ppm. Scale bar = 200 μm. $N = 6$, "*" indicates $P < 0.05$.

standard indicator of cellular injury and viability loss.[26] We observed concentration- and phase-dependent changes in morphology and viability of astrocytes in the presence of TiO_2 nanoparticles after 24 h exposure (Fig. 2A). Exposure to 100 ppm of P25 and anatase demonstrated the most profound changes in cell morphology and viability (65% and 61% loss of viability respectively), as compared to 100 ppm rutile (37%). In addition, the change in morphology, and subsequent cell viability, was concentration dependent and correlated well with the LC_{50} values with the greatest difference in P25, anatase and rutile at each concentration (Fig. 2B). Exposure to 50 ppm resulted in 50%, 39% and 34% viability loss in P25, anatase and rutile nanoparticles, respectively. Finally exposure to 25 ppm resulted in the least damage to viability with only 28%, 27% and 16% viability loss in P25, anatase and rutile, respectively. Similar results have been found in other cell lines and mixed cultures that observed reduced cell size and rounded shape prior to cell detachment.[25,26] Overall, these experiments provide strong evidence that we were working across the sub-acute toxicity range with the highest concentration of nanoparticle (100 ppm) exposure in the most lethal nanoparticles causing 65% and the lowest concentration (25 ppm) causing 28% viability loss in primary astrocytes.

2.4. TiO_2 nanoparticle exposure induces loss in glutamate uptake

To study the effect of TiO_2 nanoparticle exposure on primary astrocyte function, we measured glutamate uptake (Fig. 3). Astrocytes are the major cells of the brain to clear and process glutamate for future neuron function and prevention of neural excitotoxicity, therefore a loss of this function indicates damage to astrocytes and could have a negative effect on the overall brain health.[40,41] We observed significant concentration (25 ppm, 50 ppm, and 100 ppm) and type dependent (P25, anatase, and rutile) loss in glutamate uptake in astrocytes due to exposure to TiO_2 nanoparticles. The exposure of astrocytes to 25 ppm, 50 ppm, and 100 ppm of P25 resulted in 31%, 33% and 27% reduction in glutamate uptake, respectively. The exposure of astrocytes to 50 ppm and 100 ppm of anatase resulted in 45% and 46% reduction in glutamate uptake, respectively, while 25 ppm did not affect the glutamate uptake in astrocytes compared to untreated cells. The exposure of astrocytes to rutile resulted in a negligible reduction in glutamate uptake in 25 ppm and 50 ppm while 100 ppm resulted in 40% reduction in glutamate uptake. These data indicate that TiO_2 nanoparticle exposure exerts both concentration- and type-dependent effects on glutamate uptake of astrocytes with P25 causing the highest damage to astrocyte function even at a low concentration of 25 ppm.

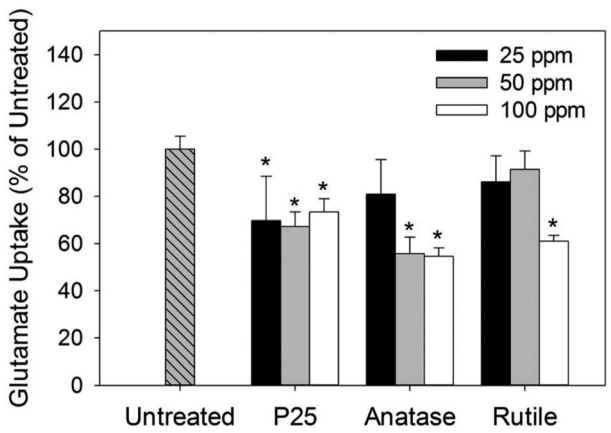

Fig. 3 Effect of TiO_2 nanoparticles on glutamate uptake. TiO_2 nanoparticle exposure resulted in decrease of glutamate uptake observed indicating loss of important cellular functions in astrocytes. $N = 3$, "*" indicates $P < 0.05$.

The ability to produce, uptake and recycle glutamate is a vital role of astrocytes in the brain as they interact with neurons for healthy brain functions.[40,41] Hence, the compromise of this function through TiO_2 nanoparticle exposure is indicative of a potentially detrimental effect to brain function and an increased risk toward the neurodegenerative process. Ze and coworkers observed significant glial proliferation, increase in glutamate content, and decrease in glutamate synthetase, a key enzyme for glutamate recycling, in mice treated for 9 months with low concentration TiO_2 nanoparticles.[42] This work provided evidence that TiO_2 nanoparticles have a direct effect in TiO_2 neurotoxicity through the inhibition of glutamate metabolism. However, with the complexity of the animal model it is not known if glutamate metabolism of astrocytes is hindered which could contribute to disruption of glutamate metabolism. We suspect that the observed *in vivo* failure of glutamate metabolism is due to the TiO_2 nanoparticle exposure that was related to the disruption in the glutamate uptake of astrocytes as demonstrated in our current study wherein we observe a significant loss in glutamate uptake specifically in astrocyte cultures in the presence of TiO_2 nanoparticles. Combining these studies provide strong evidence to indicate that further understanding of the mechanisms leading to a loss of glutamate metabolism needs to be explored due to the potential for neurodegenerative effects in the brain.

2.5. Increased reactive oxygen species and mitochondrial dysfunction induced by TiO_2 nanoparticles

To further investigate the damage caused by TiO_2 nanoparticle exposure in primary astrocytes, we determined intracellular levels of ROS when exposed to TiO_2 nanoparticles for 24 h. ROS generation has previously been observed to accompany a loss of glutamate uptake linking induced mitochondrial stress to loss of astrocyte function and could therefore be an attribute of TiO_2 nanoparticle toxicity.[43–45] Also, several studies have demonstrated that TiO_2 nanoparticles induce ROS species often leading to programmed cell death.[29,38] We observed a concentration- and type-dependent increase in ROS production (as indicated by enhanced CM-H_2DCFDA fluorescence) upon the exposure of primary astrocytes to TiO_2 nanoparticles (Fig. 4A). The exposure of astrocytes to 100 ppm

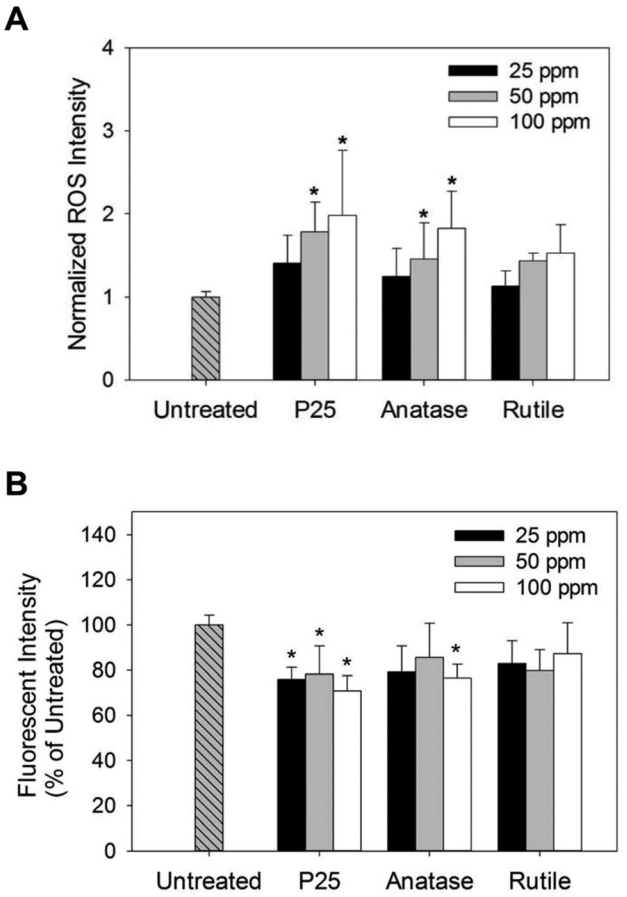

Fig. 4 Mitochondrial dysfunction. ROS generation (A) and decrease in MMP (B) indicate loss of mitochondrial health due to nanoparticle stress. $N = 5$, "*" indicates $P < 0.05$.

of P25 and anatase resulted in 1.9 ± 0.7 and 1.8 ± 0.4 fold increase in ROS production while exposure of 100 ppm of rutile did not lead to a significant ROS production, as compared to untreated cells. The higher production of ROS in P25 and anatase indicate that primary astrocytes are in a high stress environment.[46] This observation is comparable to other studies that have demonstrated a similar effect of TiO_2 nanoparticle exposure on alteration of oxidative status in both animal and cell models.[38,47]

Elevated intracellular ROS is an accepted early sign of altered mitochondrial function and can often lead to a state of mitochondrial dysfunction that has been indicated in early stages of cell death.[48] We thus investigated the effect of TiO_2 nanoparticle exposure on MMP (Fig. 4B) assessing the depolarization of mitochondrial membrane, an important marker of mitochondrial health.[26,49] We observed a 25%, 22% and 30% decrease in MMP in astrocytes exposed to P25 in 25 ppm, 50 ppm and 100 ppm, respectively, while only 100 ppm of anatase demonstrated 24% loss in MMP. Interestingly, rutile did not have a significant effect on the MMP even when exposed to 100 ppm concentration. From this data, we observed that exposure to TiO_2 nanoparticles results in type and concentration dependent mitochondrial stress leading to loss of mitochondrial health and function.

2.6. TiO_2 nanoparticle induced alteration in mitochondrial morphology

Imbalances in mitochondrial dynamics are known to impede cellular bioenergetics and contribute to numerous neurodegenerative diseases.[50] To investigate the effect of nanoparticle treatment on mitochondrial dynamics, we measured the relative gene expressions of Mfn1, Mfn2, and Drp1, markers associated with mitochondrial fusion and fission events (Fig. 5). The LC_{50} of P25, anatase and rutile TiO_2 nanoparticles are 62.37 ppm, 88.22 ppm, and 136.0 ppm, respectively. Therefore, to probe the mechanistic understanding of the changes in mitochondrial dynamics, we carried out studies here on using only 25 ppm and 100 ppm to demonstrate the drastic differences in the changes in mitochondria. We postulate that low sub-toxic concentrations (25 ppm) will cause stress resistant networks and high toxic concentrations (100 ppm) will cause mitochondrial fragmentation. 50 ppm was not utilized as this value was close to the LC_{50} value for both P25 and anatase nanoparticles which would not allow for validation of our hypothesis. Mfn1 and Mfn2 are essential proteins for the fusion process while Drp1 is an essential protein for the fission process. Changes in transcript levels of Mfn1 and Mfn2 have been reported to correlate with changes in mitochondrial dynamics.[51] Therefore we quantified the relative transcript levels in astrocytes treated with low concentration (25 ppm) and high concentration (100 ppm) to predict if astrocytes experience a perturbation in mitochondrial dynamics after 24 h treatment. Post treatment with 25 ppm of P25, we observed a 1.6 ± 0.1 and 1.5 ± 0.1 fold up-regulation of Mfn1 and Mfn2 transcripts, respectively, while no significant change in Drp1 was observed indicative of increased mitochondrial tubulation. Astrocytes treated with 25 ppm anatase and rutile also did not experience a significant increase in Drp1 (1.1 ± 0.1 and 1.2 ± 0.1, respectively) but astrocytes treated with 25 ppm anatase nanoparticles showed a significant increase in Mfn1 (1.5 ± 0.1) but not Mfn2 (1.2 ± 0.1) and astrocytes treated with 25 ppm rutile nanoparticles observed a significant increase in Mfn2 (1.5 ± 0.1) but not Mfn1 (1.3 ± 0.2). Although both Mfn1 and Mfn2 are similarly involved in the mitochondrial fusion process studies have shown that they perform unique roles and therefore the difference of upregulation observed between these treatments may explain a difference observed in mitochondrial morphology.[52] Furthermore, Tondera *et al.* observed that Mfn1 significantly contributed to mitochondrial tubulation while Mfn2 did not play a specific role and therefore we suspect that the mitochondria of astrocytes treated with 25 ppm anatase nanoparticles may be experiencing a higher degree of tubulation than those treated with 25 ppm rutile nanoparticles.[23] Astrocyte exposed to 100 ppm of P25, anatase, and rutile nanoparticles experienced significant increases in both mitofusin genes but, contrary to their 25 ppm treated counter parts, Drp1 was significantly up-regulated (2.1 ± 0.1 fold, 1.5 ± 0.1 fold and 1.6 ± 0.1 fold, respectively) which could

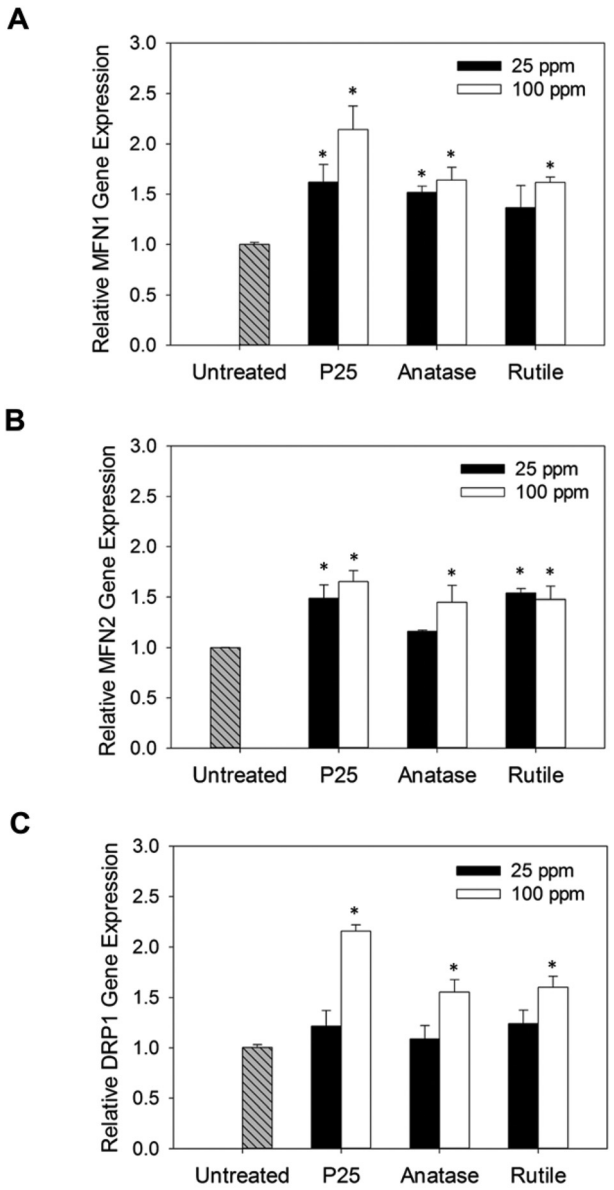

Fig. 5 Mitochondrial dynamics perturbation. Increase in Mfn1, Mfn2 and Drp1 indicate a deviation from normal mitochondrial dynamic balance toward hyperfusion in 25 ppm and 50 ppm treated cells and fission in 100 ppm treated cells. $N = 3$, "*" indicates $P < 0.05$.

indicate the activation of the fission process leading to mitochondrial fragmentation and cell death.

We further confirmed the change in dynamics by observing mitochondrial morphology utilizing confocal images (Fig. 6). The mitochondrial morphology was observed to alter in a nanoparticle and concentration dependent manner. Untreated astrocytes and 25 ppm rutile were observed to maintain similar morphology while 100 ppm rutile, 25 ppm anatase, and 25 ppm P25 treated astrocytes appear in various stages of hyperfusion. 25 ppm P25 had the greatest degree of fusion while 100 ppm rutile exhibited slight hyperfusion morphology. Mitochondria of astrocytes treated with 100 ppm P25 and anatase displayed a high degree of fragmentation. Overall the images appear to correlate well with the gene expression, especially in the P25 treated samples, however cells treated with 100 ppm rutile show a significant up-regulation in Drp1 gene expression and yet appear to maintain a slightly hyperfused mitochondria. This may reflect on the potential of gene expression as an early biomarker suggesting that a prolonged (greater than 24 h) exposure may result in fragmentation. Braydich-Stolle and co-workers used a similar strategy to demonstrate the localization and causative damage of the mitochondria due to TiO_2 nanoparticle treatment on keratinocytes.[58] Chen and co-workers utilized the mitotracker imaging to demonstrate various aspects of compromises to the disruption of the mitochondrial dynamics in cells.[59] Jou and co-workers have demonstrated similar mitochondrial morphology in primary astrocytes wherein the cells had a typical rod- or thread-like morphology without oxidative stress while oxidative stress resulted in severe fragmentation of mitochondria.[53] Our results demonstrate similar morphology changes to the mitochondria due to exposure of the nanoparticles to primary astrocytes. Further we performed acellular control experiments wherein we stained 100 ppm of P25, anatase and rutile nanoparticles with mitotracker with cells present (ESI Fig. 3†). No fluorescence was observed in these controls which demonstrated the sensitivity of the method without interference or background from nanoparticles.

Toxicity reports have consistently observed that anatase and commercially used P25 TiO_2 nanoparticles are more toxic than rutile TiO_2 nanoparticles resulting in increased tissue damage, oxidative stress and cell death.[9] This is generally understood to have roots in the difference of physicochemical properties between the two crystalline structures of nanoparticles resulting in varied interactions with the cells and environmental components.[34,54,55] In this study we demonstrated that the anatase and P25 TiO_2 nanoparticles induce concentration dependent mitochondrial dysfunction, ROS generation, and loss of astrocytic glutamate uptake. We also observed that rutile nanoparticles induced a substantial loss of glutamate uptake in the highest concentration without significant mitochondrial dysfunction and ROS generation. Many more studies have been devoted to anatase and P25 TiO_2 nanoparticles; however, the current study suggests that rutile nanoparticles can induce loss of function without induction of typical cytotoxic markers. Therefore further examination of rutile nanoparticle interaction with cells is critical in future studies.

3. Conclusions

Overall, we observed that culture of primary astrocytes with commercially and industrially relevant TiO_2 nanoparticles caused concentration- and type-dependent cytotoxic effects in primary astrocytes. In P25 and anatase TiO_2 nanoparticle treated astrocytes the glutamate uptake was significantly disrupted even at concentrations as low as 25 ppm. These altera-

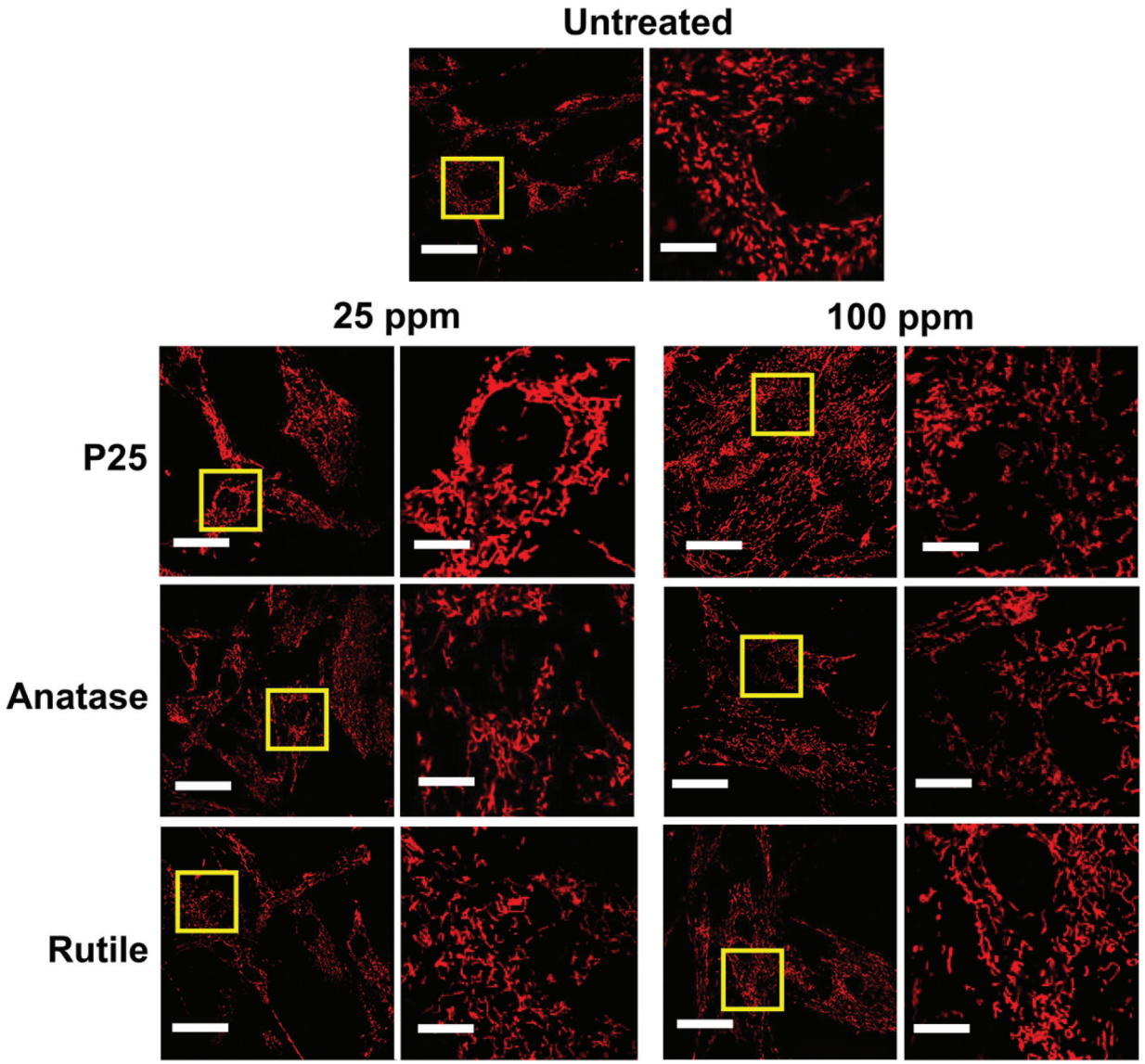

Fig. 6 Mitochondrial morphology observed by confocal fluorescent microscopy in primary rat astrocytes using MitoTracker® Red CMXRos. Scale bar 50 μm in full images. Magnified region emphasized by a gold box. Scale bar of magnified region is 12.5 μm. In the control image, long fiber-like mitochondrial morphology can be observed, as compared to fragmented and swollen mitochondria as seen in nanoparticle treated samples. Magnified region emphasized by a gold box. Scale bar of magnified region is 12.5 μm. Red is MitoTracker® Red CMXRos.

tions correlate with an increase in the amount of intracellular ROS production and significant deficits in mitochondrial activity. Finally, we demonstrated that exposure to TiO_2 nanoparticles results in significant damage to mitochondrial dynamics as seen in the up-regulation of Mfn1 and Mfn2 at 25 ppm and up-regulation of Drp1 at 100 ppm, markers indicative of the fusion and fission processes, respectively. These changes in mitochondrial morphology were further confirmed with fluorescent images of mitochondria in which 100 ppm of P25 and anatase, which significantly increased Drp1 expression, promoted fragmentation and 25 ppm of P25 and anatase resulted in various degrees of tubulation. This was not observed in cells treated with rutile TiO_2 nanoparticles which resulted in significant loss of glutamate uptake without inducing significant cell stress. From these observations, we propose that P25 and anatase TiO_2 nanoparticles induce a loss of glutamate uptake, an important astrocyte function, while the mechanisms of toxicity for rutile TiO_2 nanoparticles remain unclear. P25 and anatase TiO_2 nanoparticles induce cytotoxicity of astrocytes by (1) disrupting the mitochondrial dynamics, (2) inducing damage to the mitochondrial health and (3) fostering generation of ROS (Fig. 7). Therefore, we conclude that TiO_2 nanoparticles could potentially contribute to subsequent adverse health effects and the development of neurodegenerative diseases.

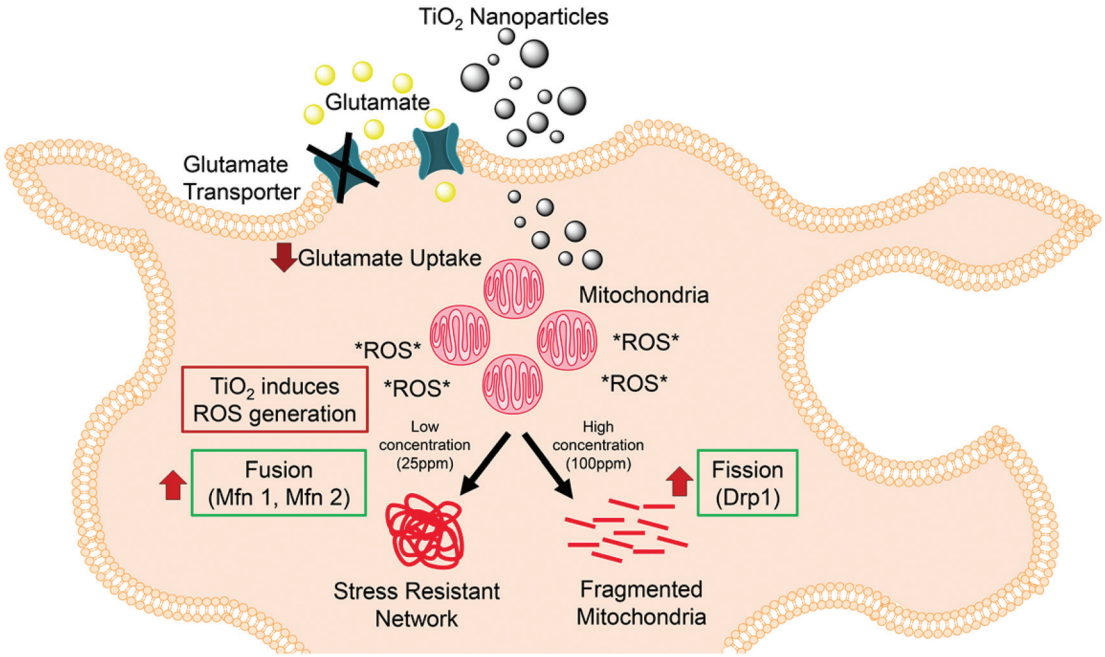

Fig. 7 Schematic representation of our postulated mechanisms mediating TiO_2 nanoparticle toxicity in astrocytes. We propose that P25 and anatase TiO_2 induces cytotoxicity and loss of functions in astrocytes through the change in intracellular oxidation state mediated by an increase of ROS production and mitochondrial dysfunction. Mitochondrial fission and fusion cycles normally consist of fission mediated by Drp1 and fusion mediated by Mfn1 and Mfn2. High concentration (100 ppm) of TiO_2 nanoparticles induces high levels of stress and mitochondrial fragmentation *via* Drp1-mediated fission. Low concentration (25 ppm) of TiO_2 nanoparticles induce low stress response, which leads to mitochondrial fusion to create stress resistant networks.

4. Experimental

4.1. Preparation of TiO_2 nanoparticle suspensions

The nanoparticles utilized for this study were Degussa P25 [Sigma Aldrich, St. Louis, MO], anatase, or rutile [Mk Nano] titanium dioxide nanoparticles. Prior to suspension all nanoparticles were sterilized by UV overnight. 1000 ppm stock suspensions were prepared in autoclaved 1× PBS by sonication [FS30D Fisher Scientific] for 30 min and stored at 4 °C. For experiments, the stock suspensions were sonicated for 30 min in culture media.

4.2. Isolation, seeding and treatment of primary astrocytes

This study was carried out in strict accordance with the recommendations in the Guide for the Care and Use of Laboratory Animals of the National Institutes of Health. The protocol was approved by the Committee on the Ethics of Animal Experiments of the University of Nebraska-Lincoln (Project ID: 1046). Primary cortical astrocytes were prepared from 1–2 day-old Sprague-Dawley rat pups of four donor rats yielding 12+ pups per litter [Charles River] in compliance with UNL's IACUC protocol 1046 and according to the protocol with slight modifications.[56,57] Briefly, the tissue was digested with 0.025% Trypsin [Life Technologies] and 0.0016% DNase [Roche] which was quenched by culture media (DMEM) [MP Biomedicals], 10% Heat Inactivated Horse Serum [PAA Lab], 1% HEPES [Media Tech], 1% penicillin–streptomycin [Life Technologies], 1% L-Glutamine [Life Technologies]). The inactive trypsin was removed by centrifugation at 1700 rpm for 5 min, and the cells were suspended in plating media and gently triturated with a glass pipette. The cells were then passed through a 70 μm cell filter, centrifuged, suspended in culture media and counted by trypan blue staining with a hemocytometer. Astrocytes were seeded on poly-L-lysine coated tissue culture plates at a density of 500 cells per mm^2. Cultures were characterized by fluorescent microscopy using anti-glial fibrillary acidic protein (GFAP) [DAKO] and 4′,6-diamidino-2-phenylindole (DAPI) nuclear stain [Thermo Scientific] yielding cultures of >90% GFAP positive cells (ESI Fig. 3†).

4.3. Nanoparticle characterization

ZetaPALS [Brookhaven instrument] was utilized to determine the nanoparticle effective diameter and Zeta potential [PALS Zeta Potential Analyzer, Smoluchowski model] at the treatment concentrations of 25 ppm, 50 ppm and 100 ppm. Nanoparticle solutions were prepared with culture media at pH 7.4 as outlined for experiments. All size measurements were performed at 25 °C and at a scattering angle of 90° and analyzed *via* intensity and volumetric distribution. Nanoparticles were suspended in deionized water visualized with a Hitachi H7500 Transmission Electron Microscope on carbon coated copper grids [Ted Pella].

4.4. Lethal concentration assay using MTT

The concentration lethal to 50% of astrocytes (LC_{50}) was determined utilizing the MTT [3-(4,5-dimethyldiazol-2-yl)2,5 diphenyl tetrazolium bromide] [Life Technologies] assay. It is a colorimetric assay that evaluates the mitochondrial conversion of the MTT salt. In short, after 24 h nanoparticle exposure the culture media was aspirated and 5 mg ml^{-1} MTT working solution in DMEM incubated on live cells at 37 °C for 3 h. Lysis buffer (0.1 N HCl in isopropanol) was added in a 5 : 1, lysis buffer to MTT solution, ratio. The absorbance values were read at 570/630 nm in an AD340 plate reader [Beckman Coulter]. The 570/630 nm absorbance ratio values were imputed into Sigma plot [Systat Software] and LC_{50} values determined utilizing regression wizard and a four parameter logistic curve.

4.5. Phase imaging

Morphology of live cells were assessed using an Axiovert 40 CFL [Zeiss] and images taken with a Progres C3 [Jenoptik] camera.

4.6. Reactive oxygen species (ROS) quantification

5-(and-6)-Chloromethyl-2′,7′-dichlorodihydrofluorescein diacetate (CM-H_2DCFDA) is a fluorescent indicator activated by the presence of ROS. The culture media was aspirated and the cells were washed with warm 1× PBS. 10 μM CM-H_2DCFDA [Life Technologies] in DMEM was added to each well and incubated at 37 °C for 30 min. Cells were washed 3× with PBS followed by fluorobrite media [Life Technologies] added to each well. The bottom of the well was read at excitation 495 nm and emission 529 nm with a SLFA plate reader [Biotek]. The results were reported as a fraction of the average untreated intensity.

4.7. Glutamate uptake assay

The uptake of [3H] glutamic acid was used to determine change in glutamate uptake experienced by TiO_2 nanoparticle treated astrocytes. The treatment media was removed and replaced by serum free high glucose DMEM containing 50 μM glutamate and 18.5 kBq of [3H] glutamic acid [Perkin Elmer]. The uptake was terminated after 15 min by removal of working solution. Cells were washed twice with ice-cold PBS lysed in 10 mM NaOH containing 0.1% Triton X-100, and 300 μl of lysate was assayed for [3H] by liquid scintillation counting. The protein content was assayed using the Bradford assay. Results were reported as CPM per μg protein.

4.8. Mitochondrial membrane potential (MMP)

MMP was determined using tetramethylrhodamine (TMRM) [Life Technologies], a cationic red dye which accumulates in healthy, active mitochondria marking depolarization. The stock solution was diluted in fluorobrite DMEM to a final concentration of 20 nM, added to cells, and incubated in the dark at room temperature for 45 min. Afterwards, the dye was removed and cells were washed 3× with warm 1× PBS. The fluorescence was read at emission 590 nm and excitation 573 nm. Results are reported as the normalized intensity to the untreated cells.

4.9. Gene expression

Total RNA was isolated using Trizol [Life Technologies] according to the manufacturer's instructions. The quality and quantity was determined by using a ND-1000 spectrophotometer [NanoDrop Technologies] and reverse transcribed using an iSciptTM cDNA synthesis kit [Bio-Rad Laboratories] according to the manufacturer's instructions.

Quantitative real time PCR was performed using SYBR Green Master Mix [Applied Biosystems, Foster City, CA] in an ep gradient S Mastercycler [Eppendorf]. The PCR program was set as follows: 10 min at 95 °C, 40–60 cycles of 95 °C for 15 s followed by annealing at 60 °C for 15 s and elongation at 72 °C for 60 s, and finally 95 °C for 15 s to end. The primers of interest obtained from Integrated NDA Technologies [Coralville, IA] with the following sequences: GLAST (forward 5′-CTACTCACCGTCAGCGCTGT-3′ and reverse 5′-AGCACAAATCTGGTGATGCG-3′), Mfn1 (forward 5′-TCGTGCTGGCAAAGAAGG-3′ and reverse 5′-CGATCAAGTTCCGGGTTCC-3′), Mfn2 (forward 5′-CGATGTGGTAGTGAGGTTGG-3′ and reverse 5′-CTCCCATCTTCCACCATTCC-3′), Drp1 (forward 5′-GAACTACCTTCCGCTGTATCG-3′ and reverse 5′-CGACCACCATCTCCAATTCC-3′). GAPDH (forward 5′-ATG ATT CTA CCC ACG GCA AG-3′ and reverse 5′-CTG GAA GAT GGT GAT GGG TT-3′) was measured as the reference. The ΔΔCT method was utilized for analysis of each sample. Results reported as normalized to the average expression of untreated cells.

4.10. Mitochondrial imaging

Mitochondrial morphology was visualized utilizing MitoTracker® Red CMXRos [Life Tech] according to manufacturer's instructions. In short, after 24 h the culture media was removed and replaced with serum free DMEM containing a 300 nM MitoTracker® probe and incubated at 37 °C for 30 min. Cells were then washed three times with warm 1× PBS and serum free DMEM was added for viewing with an Olympus FV500 Inverted Confocal Microscope.

4.11. Statistical analysis

All data are presented as the mean ± standard deviation. Statistical comparisons between treatments utilized Sigma Plot ANOVA (Dunnett's method) for analysis. Pool sizes are as indicated.

Acknowledgements

We thank Dr Yusong Li for access to the DLS machine. We thank Dr You Zhou and Han Chen of the UNL Center for Biotechnology Microscopy Core Faculties for assistance in obtaining confocal and TEM images. We thank Dr Concetta Dirusso for the use of her fluorescent plate reader. We thank

Dr William Velander for the use of his colorimetric spectrometer. We thank Dr Edward Harris for assistance in the glutamate uptake studies. This work was funded by NIH grants P30 GM103335 (to the Nebraska Redox Biology Center) and 1R01GM108975 (to O.K.), the start up funds from UNL's Layman Award, MRSEC Seed Grant and UNL Interdisciplinary Award (to S.K.) and UNL's Molecular Mechanisms of Diseases Graduate Fellowship (to C.L.W.).

References

1 F. Piccinno, F. Gottschalk, S. Seeger and B. Nowack, *J. Nanopart. Res.*, 2012, **14**, 1–11.
2 W. Thies and L. Bleiler, *Alzheimer's Dementia*, 2013, **9**, 208–245.
3 A. Weir, P. Westerhoff, L. Fabricius, K. Hristovski and N. von Goetz, *Environ. Sci. Technol.*, 2012, **46**, 2242–2250.
4 I. Iavicoli, V. Leso and A. Bergamaschi, *J. Nanomater.*, 2012, **2012**, 36.
5 T. Xia, R. F. Hamilton, J. C. Bonner, E. D. Crandall, A. Elder, F. Fazlollahi, T. A. Girtsman, K. Kim, S. Mitra, S. A. Ntim, G. Orr, M. Tagmount, A. J. Taylor, D. Telesca, A. Tolic, C. D. Vulpe, A. J. Walker, X. Wang, F. A. Witzmann, N. Wu, Y. Xie, J. I. Zink, A. Nel and A. Holian, *Environ. Health Perspect.*, 2013, **121**, 683–690.
6 J. C. Bonner, R. M. Silva, A. J. Taylor, J. M. Brown, S. C. Hilderbrand, V. Castranova, D. Porter, A. Elder, G. Oberdorster, J. R. Harkema, L. A. Bramble, T. J. Kavanagh, D. Botta, A. Nel and K. E. Pinkerton, *Environ. Health Perspect.*, 2013, **121**, 676–682.
7 J. Wang, G. Zhou, C. Chen, H. Yu, T. Wang, Y. Ma, G. Jia, Y. Gao, B. Li and J. Sun, *Toxicol. Lett.*, 2007, **168**, 176–185.
8 J. Wang, C. Chen, Y. Liu, F. Jiao, W. Li, F. Lao, Y. Li, B. Li, C. Ge, G. Zhou, Y. Zhao and Z. Chai, *Toxicol. Lett.*, 2008, **183**, 72–80.
9 J. Wu, J. Sun and Y. Xue, *Toxicol. Lett.*, 2010, **199**, 269–276.
10 T. C. Long, N. Saleh, R. D. Tilton, G. V. Lowry and B. Veronesi, *Environ. Sci. Technol.*, 2006, **40**, 4346–4352.
11 P. J. Magistretti, *J. Exp. Biol.*, 2006, **209**, 2304–2311.
12 A. Panatier, D. T. Theodosis, J.-P. Mothet, B. Touquet, L. Pollegioni, D. A. Poulain and S. H. R. Oliet, *Cell*, 2006, **125**, 775–784.
13 V. Lebon, K. F. Petersen, G. W. Cline, J. Shen, G. F. Mason, S. Dufour, K. L. Behar, G. I. Shulman and D. L. Rothman, *J. Neurosci.*, 2002, **22**, 1523–1531.
14 L. Pellerin and P. J. Magistretti, *Proc. Natl. Acad. Sci. U. S. A.*, 1994, **91**, 10625–10629.
15 A. Araque, G. Carmignoto, P. G. Haydon, S. H. R. Oliet, R. Robitaille and A. Volterra, *Neuron*, 2014, **81**, 728–739.
16 M. Navarrete, G. Perea, L. Maglio, J. Pastor, R. Garcia de Sola and A. Araque, *Cereb. Cortex*, 2013, **23**, 1240–1246.
17 A. Araque, *Neuron Glia Biol.*, 2008, **4**, 3–10.
18 A. Volterra and J. Meldolesi, *Nat. Rev. Neurosci.*, 2005, **6**, 626–640.
19 E. A. Newman, *Trends Neurosci.*, 2003, **26**, 536–542.
20 V. Freyre-Fonseca, N. L. Delgado-Buenrostro, E. B. Gutierrez-Cirlos, C. M. Calderon-Torres, T. Cabellos-Avelar, Y. Sanchez-Perez, E. Pinzon, I. Torres, E. Molina-Jijon, C. Zazueta, J. Pedraza-Chaverri, C. M. Garcia-Cuellar and Y. I. Chirino, *Toxicol. Lett.*, 2011, **202**, 111–119.
21 Y. Tang, F. Wang, C. Jin, H. Liang, X. Zhong and Y. Yang, *Environ. Toxicol. Pharmacol.*, 2013, **36**, 66–72.
22 R. J. Youle and A. M. Van Der Bliek, *Science*, 2012, **337**, 1062–1065.
23 D. Tondera, S. Grandemange, A. Jourdain, M. Karbowski, Y. Mattenberger, S. Herzig, S. Da Cruz, P. Clerc, I. Raschke and C. Merkwirth, *EMBO J.*, 2009, **28**, 1589–1600.
24 J. Yang, Q. Liu, M. Qi, S. Lu, S. Wu, Q. Xi and Y. Cai, *Environ. Toxicol.*, 2013, **28**, 489–497.
25 A. Gramowski, J. Flossdorf, K. Bhattacharya, L. Jonas, M. Lantow, Q. Rahman, D. Schiffmann, D. G. Weiss and E. Dopp, *Environ. Health Perspect.*, 2010, **118**, 1363.
26 S. G. Márquez-Ramírez, N. L. Delgado-Buenrostro, Y. I. Chirino, G. Gutiérrez-Iglesias and R. López-Marure, *Toxicology*, 2012, **302**, 146–156.
27 L. Shang, K. Nienhaus and G. U. Nienhaus, *J. Nanobiotechnol.*, 2014, **12**, 5.
28 R. Tedja, M. Lim, R. Amal and C. Marquis, *ACS Nano*, 2012, **6**, 4083–4093.
29 T. C. Long, J. Tajuba, P. Sama, N. Saleh, C. Swartz, J. Parker, S. Hester, G. V. Lowry and B. Veronesi, *Environ. Health Perspect.*, 2007, **115**, 1631.
30 J. A. Kim, A. Salvati, C. Aberg and K. A. Dawson, *Nanoscale*, 2014, **6**, 14180–14184.
31 R. Y. Prasad, K. Wallace, K. M. Daniel, A. H. Tennant, R. M. Zucker, J. Strickland, K. Dreher, A. D. Kligerman, C. F. Blackman and D. M. DeMarini, *ACS Nano*, 2013, **7**, 1929–1942.
32 F. Wang, L. Yu, M. P. Monopoli, P. Sandin, E. Mahon, A. Salvati and K. A. Dawson, *Nanomedicine*, 2013, **9**, 1159–1168.
33 A. Lesniak, F. Fenaroli, M. P. Monopoli, C. Aberg, K. A. Dawson and A. Salvati, *ACS Nano*, 2012, **6**, 5845–5857.
34 A. Marucco, I. Fenoglio, F. Turci and B. Fubini, Journal of Physics: Conference Series; IOP Publishing, *Interaction of fibrinogen and albumin with titanium dioxide nanoparticles of different crystalline phases*, 2013, p. 012014.
35 Y. Li, J. Li, J. Yin, W. Li, C. Kang, Q. Huang and Q. Li, *J. Nanosci. Nanotechnol.*, 2010, **10**, 8544–8549.
36 I. Iavicoli, *Eur. Rev. Med. Pharmacol. sci.*, 2011, **15**, 481–508.
37 S. Wang, H. Yu and J. K. Wickliffe, *Toxicol. In Vitro*, 2011, **25**, 2147–2151.
38 E. Huerta-García, J. A. Pérez-Arizti, S. G. Márquez-Ramírez, N. L. Delgado-Buenrostro, Y. I. Chirino, G. Gutiérrez-Iglesias and R. López-Marure, *Free Radicals Biol. Med.*, 2014, **73**, 84–94.
39 J. Gordon, S. Amini and M. K. White, in *Neuronal Cell Culture*, Springer, 2013, pp. 1–8.
40 L. Hertz and H. R. Zielke, *Trends Neurosci.*, 2004, **27**, 735–743.

41 N. J. Maragakis and J. D. Rothstein, *Nat. Clin. Pract. Neurol.*, 2006, **2**, 679–689.
42 Y. Ze, R. Hu, X. Wang, X. Sang, X. Ze, B. Li, J. Su, Y. Wang, N. Guan and X. Zhao, *J. Biomed. Mater. Res. Part A*, 2014, **102**, 470–478.
43 A. Volterra, D. Trotti, C. Tromba, S. Floridi and G. Racagni, *J. Neurosci.*, 1994, **14**, 2924–2932.
44 O. Sorg, T. Horn, N. Yu, D. L. Gruol and F. E. Bloom, *Mol. Med.*, 1997, **3**, 431.
45 C. Yuan, J. Gao, J. Guo, L. Bai, C. Marshall, Z. Cai, L. Wang and M. Xiao, *PloS One*, 2014, **9**, e107447.
46 N. S. Chandel, *BMC Biol.*, 2014, **12**, 34.
47 J. Shin, E. Lee, S. Seo, H. Kim, J. Kang and E. Park, *Neuroscience*, 2010, **165**, 445–454.
48 M. D. Brand and D. G. Nicholls, *Biochem. J.*, 2011, **435**, 297–312.
49 S. Hussain, K. Hess, J. Gearhart, K. Geiss and J. Schlager, *Toxicol. in Vitro*, 2005, **19**, 975–984.
50 K. Itoh, K. Nakamura, M. Iijima and H. Sesaki, *Trends Cell Biol.*, 2013, **23**, 64–71.
51 J. J. Rahn, K. D. Stackley and S. S. Chan, *PLoS One*, 2013, **8**, e59218.
52 S. Cipolat, O. M. de Brito, B. Dal Zilio and L. Scorrano, *Proc. Natl. Acad. Sci. U. S. A.*, 2004, **101**, 15927–15932.
53 M. J. Jou, T. I. Peng, R. J. Reiter, S. B. Jou, H. Y. Wu and S. T. Wen, *J. Pineal Res.*, 2004, **37**, 55–70.
54 Z. E. Allouni, P. J. Høl, M. A. Cauqui, N. R. Gjerdet and M. R. Cimpan, *Toxicol. In Vitro*, 2012, **26**, 469–479.
55 M. Czajka, K. Sawicki, K. Sikorska, S. Popek, M. Kruszewski and L. Kapka-Skrzypczak, *Toxicol. In Vitro*, 2015, **29**, 1042–1052.
56 G. M. Beaudoin III, S.-H. Lee, D. Singh, Y. Yuan, Y.-G. Ng, L. F. Reichardt and J. Arikkath, *Nat. Protoc.*, 2012, **7**, 1741–1754.
57 S. Kidambi, I. Lee and C. Chan, *Adv. Funct. Mater.*, 2008, **18**, 294–301.
58 L. K. Braydich-Stolle, N. M. Schaeublin, R. C. Murdock, J. Jiang, P. Biswas, J. J. Schlager and S. M. Hussain, *J. Nanopart Res.*, 2009, **11**, 1361–1374.
59 H. Chen, A. Chomyn and D. C. Chan, *J. Biol. Chem.*, 2005, **280**, 26185–26192.

Electronic Supplementary Material (ESI) for Nanoscale.

Mitochondrial Dysfunction and Loss of Glutamate Uptake in Primary Astrocytes Exposed to Titanium Dioxide Nanoparticles

Christina L. Wilson[1], Vaishaali Natarajan[1], Stephen L. Hayward[1], Oleh Khalimonchuk[2], and Srivatsan Kidambi[1,3,4,*]

[1]Department of Chemical and Biomolecular Engineering,

University of Nebraska-Lincoln, NE, 68588

[2]Department of Biochemistry and Nebraska Redox Biology Center,

University of Nebraska-Lincoln, NE, 68588

[3]Nebraska Center for Materials and Nanoscience,

University of Nebraska-Lincoln, NE, 68588

[4]Regenerative Medicine Program,

University of Nebraska Medical Center, NE, 68198.

[*]indicates corresponding author. Email: skidambi2@unl.edu

SUPPLEMENTARY INFORMATION

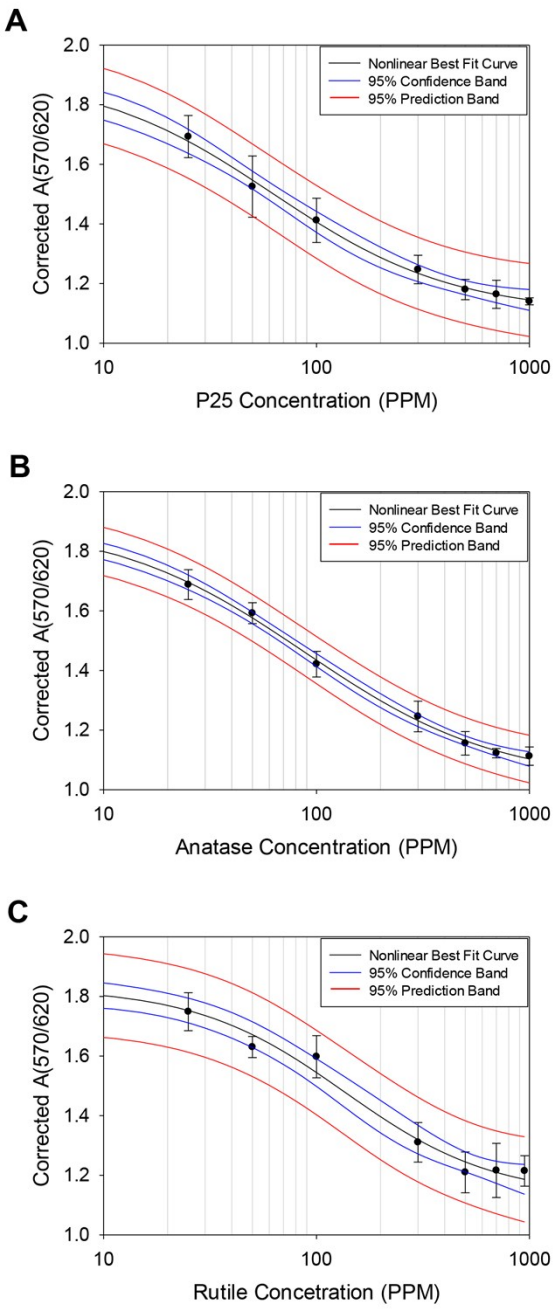

Suppl Fig 1. Lethal Concentration. Lethal concentration was quantified at 0ppm, 25ppm, 50ppm, 100ppm, 300ppm, 500ppm, 700ppm and 1000ppm nanoparticle. P25 (A) was observed to be the most lethal nanoparticle after 24 hr treatment followed by anatase (B) and rutile (C) as determined by calculating the LC_{50} utilizing sigma plot analysis. (N = 6).

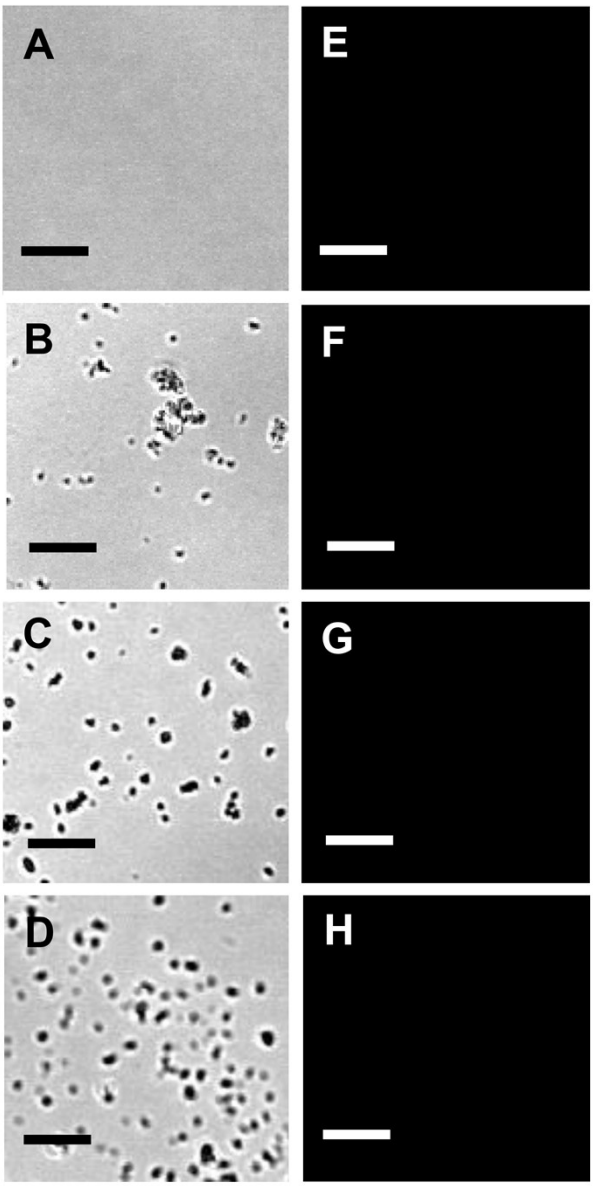

Suppl Fig 2. Acellular stained images of TiO_2 nanoparticles with MitoTracker Red. Confocal phase (A-D) and florescent (E-H) images of no nanoparticles (A,E), 100 ppm P25 (B,F), 100 ppm Anatase (C, G) and 100 ppm Rutile (D,H) nanoparticles treated with 300 nM MitoTrackerR Red CMXROS dye as described in the experimental section. Scale bar 10 μm.

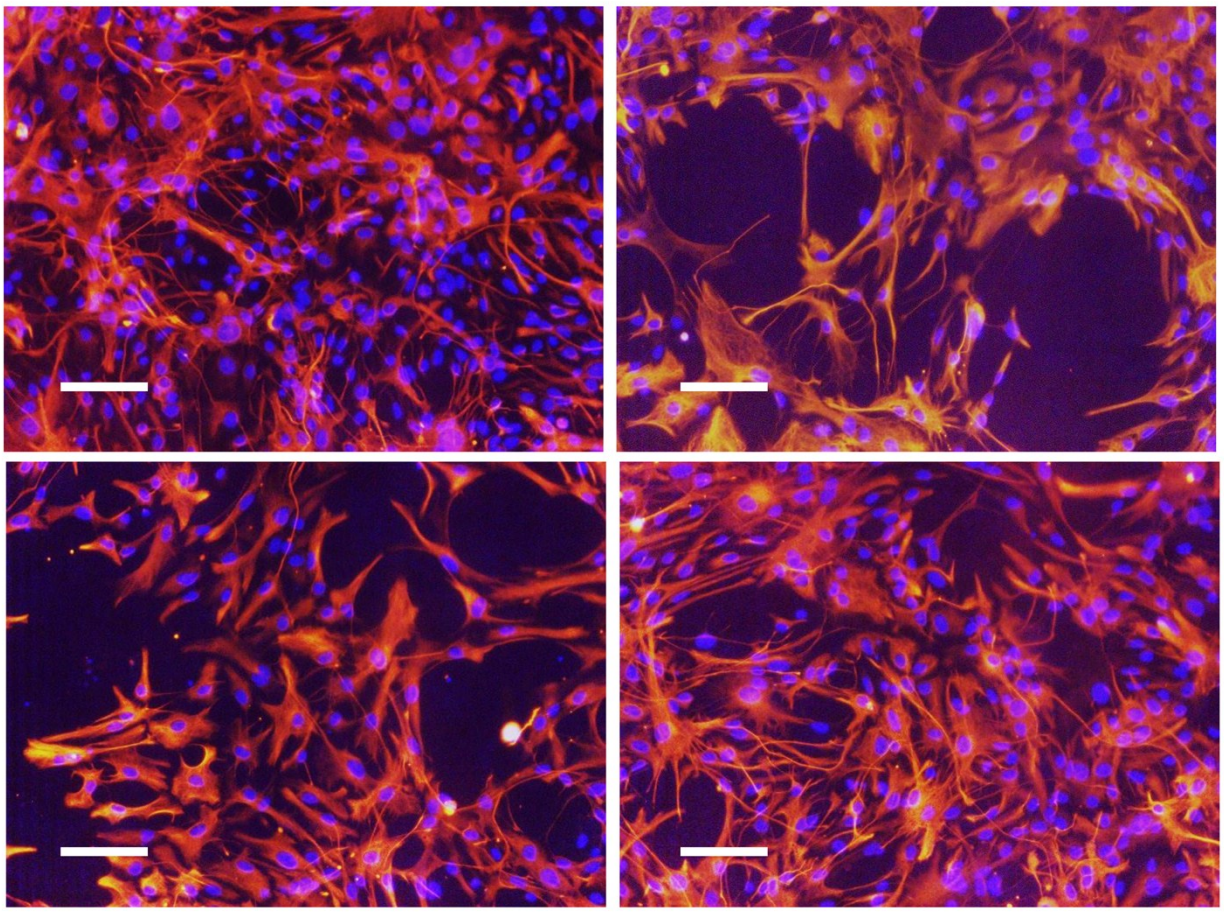

Suppl Fig 3. Representative images of the untreated astrocyte culture. The astrocyte culture utilized for experiments was characterized by immunostaining with anti-glial fibrillary acidic protein (GFAP, red) and DAPI nuclear staining (blue). Cells were fixed with 4% paraformaldehyde for 20 min, permeabilized in 0.1% Triton X-100 for 15 min and background blocked with 1% bovine serum albumin (BSA) in PBS for 1 hr at room temperature. Cells were stained in primary antibody solution (1:1000 anti-GFAP [DAKO] in 1% BSA in PBS) at 4 °C overnight, secondary antibody solution (1:500 anti-Rabbit rhodamine [Millipore] in PBS) for 2 hr at room temperature and DAPI staining solution (1 µg/ml DAPI in PBS) for 5 min at room temperature. Images were obtained using Axiovert 40 CFL [Zeiss] and images taken with a Progres C3 [Jenoptick] camera with an X-Cite series 120Q [Lumen Dynamics] lamp and a CY3 or DAPI filter [Chroma]. Culture purity was determined to be > 90 % astrocytes by counting the number of GFAP positive nuclei over the total nuclei using Image J cell counter [NIH.gov].